

Nested economies of scale in city mass

Kangning Huang^{1,2*}, Mingzhen Lu^{3*}

Author affiliations:

¹Shanghai Key Laboratory of Urban Design and Urban Science, NYU Shanghai, Shanghai 200124, China

²Division of Arts and Sciences, NYU Shanghai, Shanghai 200124, China

³Department of Environmental Studies, New York University, New York, NY 10003, USA

*Both authors contributed equally

E-mail addresses (ORCID):

K. Huang: kangning.huang@nyu.edu (0000-0001-6877-9442);

M. Lu: mingzhen.lu@nyu.edu (0000-0002-8707-8745);

Keywords: city mass, built environment, scaling theory, sustainability, complex system, economies of scale, sublinearity, zipf's law

Corresponding authors:

Kangning Huang,
Division of Arts and Sciences,
New York University Shanghai,
567 West Yangsi Road, Shanghai, China
Email: kangning.huang@nyu.edu

Mingzhen Lu,
Department of Environmental Studies
New York University,
59 Washington Square East, New York, NY 10003, USA
Email: mingzhen.lu@nyu.edu

Abstract

A longstanding puzzle in urban science is whether there's an intrinsic match between human populations and the mass of their built environments. Previous findings have revealed various urban properties scaling nonlinearly with population, yet existing models of city built mass are still dominated by per-capita linear thinking. Our analysis of >3,000 cities globally reveals universal sublinear scaling of city mass with population at both the city ($\beta=0.90$) and neighborhood levels ($\delta=0.75$). This means that larger cities and denser neighborhoods achieve economies of scale with less per-capita city mass. Our theoretical framework further shows that city-level scaling emerges naturally from within-city disparities. This multi-scale understanding redefines "over-built" and "under-built" conditions as deviations from expected scaling patterns, implying either excessive environmental impacts or inadequate living standards. Effective urban policy thus requires moving beyond simple per-capita assumptions, adopting scale-adjusted metrics and managing cities as nested, complex systems.

Main text

A key feature of human life is the extensive transformation of Earth's materials into built structures, establishing the biophysical foundation of modern civilization (1–3). This capacity to harness external mass has progressively intensified since the Stone Age, evolving from simple makeshift shelters in early human settlement (4) into today's complex city built mass (5), where individuals find comfort and protection within individual buildings, enjoy local conveniences like grocery shopping and schooling within vibrant neighborhoods, and traverse city-wide networks for professional collaborations and cultural exchanges (6).

Recent studies (3, 7, 8) indicate that global per-capita built mass has grown exponentially, with an approximate annual growth rate of 1.8% over the past 120+ years (Fig.1A, Methods). In 1900, per-capita built mass worldwide was already considerable at 22 tonnes per person, and has since increased nearly tenfold to 205 tonnes per person today. Concurrently, per-capita vegetation biomass (dry weight) has decreased substantially from 694 tonnes to 138 tonnes. Expressed dimensionless relative to average human body mass (~50 kg, Methods), each person now corresponds to about 4,090× their body mass in built mass and 2,760× in vegetation biomass (Fig.1A).

The UN projects a global urban population increase of over 2 billion by 2050 (9), requiring significant expansion of built infrastructure in cities. This growth, combined with increasing material use per capita driven by rising living standards, is projected (10) to drive annual material use for urban construction and maintenance from 40 billion tonnes in 2010 to about 90 billion tonnes by 2050.

However, this projection has two key limitations: 1) It relies on linear models, implicitly assuming that per-capita material consumption depends solely on living standards and affluence (11), independent of city size. Recent advances in urban scaling research (12–14) challenges this assumption, showing that many urban properties scale nonlinearly with city size, making per-capita predictions questionable. 2) It lacks spatial detail, overlooking significant variations in infrastructure within cities (15–17). This limits insight into whether nonlinear scaling holds across spatial scales, from cities to neighborhoods. These gaps—linear assumptions and low spatial resolution—hinder accurate predictions of material use and infrastructure needs across diverse urban areas, risking misguided sustainability and climate policies.

Here we utilize high-resolution mappings of buildings (18–20), mobility infrastructure (21), and pavement (22) in >3,000 cities (23) worldwide (Fig.1B, Fig.S1,4-6, SI Methods) and region/type-specific material intensities (24, 25), to characterize the mass distribution of the human built stock.

Our analysis offers an in-depth look of the built-structure vs. human match in urban settings. The total built mass of cities worldwide is a staggering 324 gigatonne, equivalent to every inch of global urban impervious area (22) (~0.3M km²) submerged under half meter deep of solid concrete (height of a coffee table). All cities taken together, each person is supported by built structure—buildings and mobility infrastructure such as paved roads and parking lots—that is >5,000 times their own mass while only enjoying vegetation 64 times of their mass (Fig.1C). This finding suggests that albeit more densely built, urban built structure vs. human match is on par with the global average (~4,000×), but urban systems have dramatically less vegetation per person (64× vs. 2,768× global average).

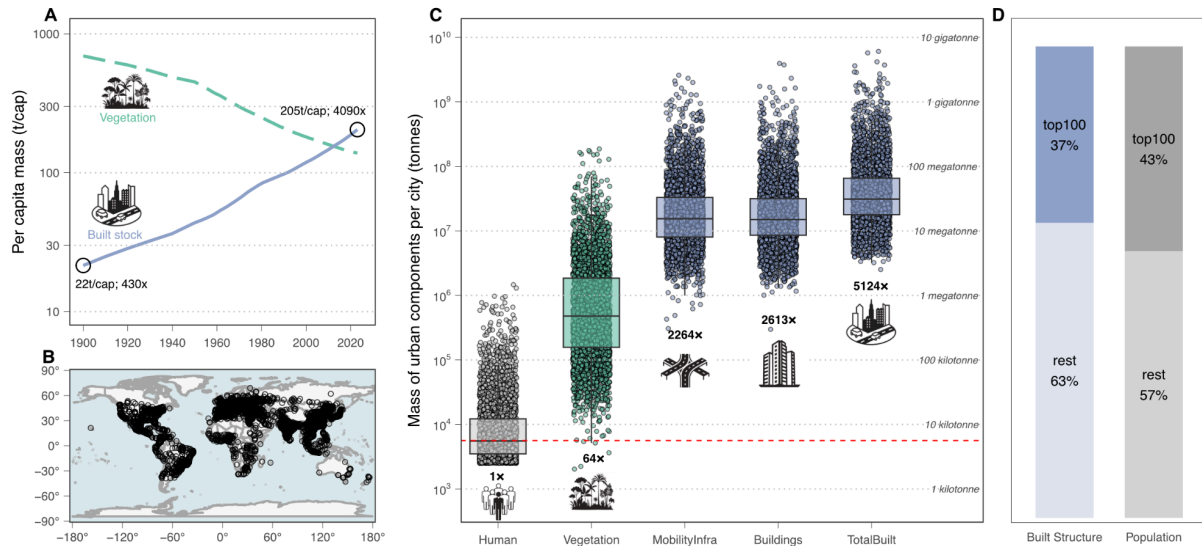


Figure 1| Global mass distribution of the built stock in relation to vegetation and humans.

(A), Per-capita built stock increased exponentially from 22t/cap in 1900 to 205t/cap today, a 1.8% annual growth. In contrast, per-capita vegetation biomass declined from 694t/cap to 138t/cap, a 1.3% annual decrease. Note that the y axis is logarithmic scale. (B) Map of 3593 cities included in our analysis with a size cutoff of 50,000 residents (Methods). (C) City-level mass of the built environment is ranked according to the median value: Human (gray), vegetation biomass (green), mobility infrastructure (blue), buildings (blue), total built stock (blue). The red dashed line (median city-level human mass) serves as a reference threshold across categories. Scale indicators below each category (e.g., 64 \times) denote the average multiplicative difference relative to human mass (average human body mass estimated to be 50kg), highlighting the magnitude of resources required to support human living. (D) The world's biggest 100 cities account for 37% of all mass and 43% of urban population. In each box plot, the lower and upper bounds of the whiskers denote minima and maxima, the center line denotes the median, and the lower and upper bounds of the boxes represent the 25% and 75% quantiles, respectively.

Looking beyond per-cap averages, the distribution of city mass is highly right-skewed (Fig.1D): the world's heaviest 100 cities—less than 3% of all cities—alone account for ~37% of all urban mass, equivalent to the mass of the smallest 3,314 cities combined (~90% of cities). The distribution of population is similarly more concentrated in big cities: the top 100 populous cities alone host 43 % of the global urban population. Curiously, the top 100 most populous cities in the world host more share of population with disproportionately less built mass, resulting in an approximately 32% lower per capita built mass compared to the rest of the world (172 vs. 252 t/cap).

This notable difference suggests that the per-capita ratio may not be scale-invariant and could potentially decline as cities grow larger. In the next section, we analyze the nonlinear dependence of built stock as a function of city size.

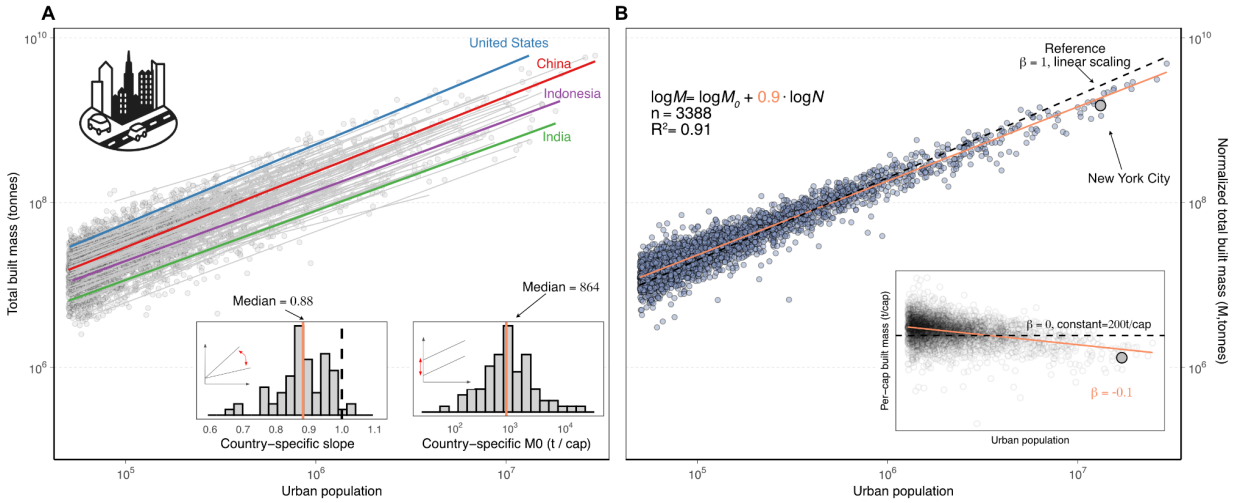


Figure 2| Sublinear urban scaling of built mass and variations are universal. (A) Log-log scatter plot of total city mass (tonnes) scales sublinearly with population across cities (gray dot) from 74 countries, indicating economies of scale in urban infrastructure materials. A country is included if they have more than 5 cities. We colored 4 countries to highlight similarity of slopes and variations of intercept. All other countries are denoted by gray lines (see Fig.S2 for regressions of all countries and Fig.S3 for distribution of goodness of fit). Inset on the left describes the distribution of country-specific scaling slope ($n=74$, median=0.88), while inset on the right describes the distribution of country-specific intercept M_0 ($n=74$, median = 864 t/cap $^\beta$). **(B)** After normalizing cities based on their country-specific intercepts, the solid orange line shows the best-fit power-law scaling relationship (exponent $\beta = 0.9$, $R^2 = 0.91$, $n = 3,388$). The dashed black line represents the linear expectation if city mass were directly proportional to population size based on per-capita average ($\beta = 1$). The inset highlights the divergence between these two lines expressed as per-capita built mass, underscoring the inadequacy of linear estimates. By definition of per-capita metric, $\beta=0.9-1 = -0.1$. Each blue dot represents a unique city based on our definition (Fig.S1); we highlighted New York City as an example.

It takes size to share: universal across-city economies of scale

We found a consistent sublinear scaling law between urban built structure mass and city size measured by population across major countries of the world (Fig.2A), pointing to economies of scale in material use as cities get bigger. Most countries have a scaling slope (β) around 0.88 (<1 , sublinear) despite the extreme range of economic development level, technology, culture and tradition of building style, climatic and topological features, abundance of natural resources included in our global datasets. The distribution of scaling slopes (Fig.2A, left inset) suggests that there's a central tendency of the urban system around 0.88, and country-scale variations generate deviations around this central tendency in a Gaussian manner.

However, the “elevation” of the scaling law, largely defined by the intercept of the regression, has a right-skewed distribution: some developed economies have extremely large value while underdeveloped countries have very small value. This country-scale variance in intercept seems to follow a log-normal distribution (Fig.2A, right inset, median = 864 t/cap $^\beta$), reflecting wide variations in baseline built environment mass across countries, influenced by factors such as income levels, construction practices, and historical development patterns.

Given the centralized distribution of scaling slope, we were able to normalize our city data by removing country-specific variations in “elevation” to characterize the general relationship between built stock and city size (SI Methods). We found a universal sublinear scaling law across all cities in our dataset (Fig.2B,

$\beta = 0.9$, 95% CI = (0.89,0.91), $r^2 = 0.91$, $n = 3,588$, $P < 0.001$). A city with twice the population of another city only needs 84% more mass, a 16% efficiency gain for every doubling of population size.

As a consequence, per-capita built stock mass declines as cities get bigger (by definition of “per-capita”, $\beta = 0.9 - 1 = -0.1$, Fig.2B inset), a city that is 10-times bigger is only about $\frac{3}{4}$ in per-capita mass compared to the smaller city. As cities grow, they require proportionally less built environment mass per capita, confirming that per-capita is not scale-invariant and is not a good metric to use when comparing against cities of different sizes (see contrast between dashed black and orange solid lines in Fig.2B).

The efficiencies are largely attributed to the shared use of infrastructure in larger urban areas. As cities grow, they facilitate the communal utilization of resources such as roads, utilities, and public spaces, leading to economies of scale that reduce the per capita built mass. This phenomenon aligns with the concept of urbanization economies (26, 27), where the concentration of population and activities in urban centers enhances productivity and resource efficiency through shared infrastructure and services. These findings extend previous studies on urban scaling (12, 28, 29), which demonstrated that the lengths of infrastructure—such as roads, cables, and pipes—scale sublinearly with population due to the increasing efficiency of spatial connectivity in larger urban systems.

However, previous studies have largely focused on the geometry (29–31) (*e.g.*, length or area) of infrastructure rather than its material embodiment. Our analysis introduces a new dimension: the total mass of the built environment, which offers a more direct account of the material and energetic investments embedded in infrastructure.

While these results underscore the universality of sublinear scaling at the city level, they prompt further inquiry into whether similar patterns hold within cities themselves. Despite recognition of cities displaying self-similar features at various spatial scales, previous efforts of urban scaling analysis have largely assumed cities to be homogenous. In the next section, we turn to an analysis of urban neighborhoods—a finer spatial scale that has received comparatively less attention in scaling research—to examine how built environment mass scales with population at this more granular level.

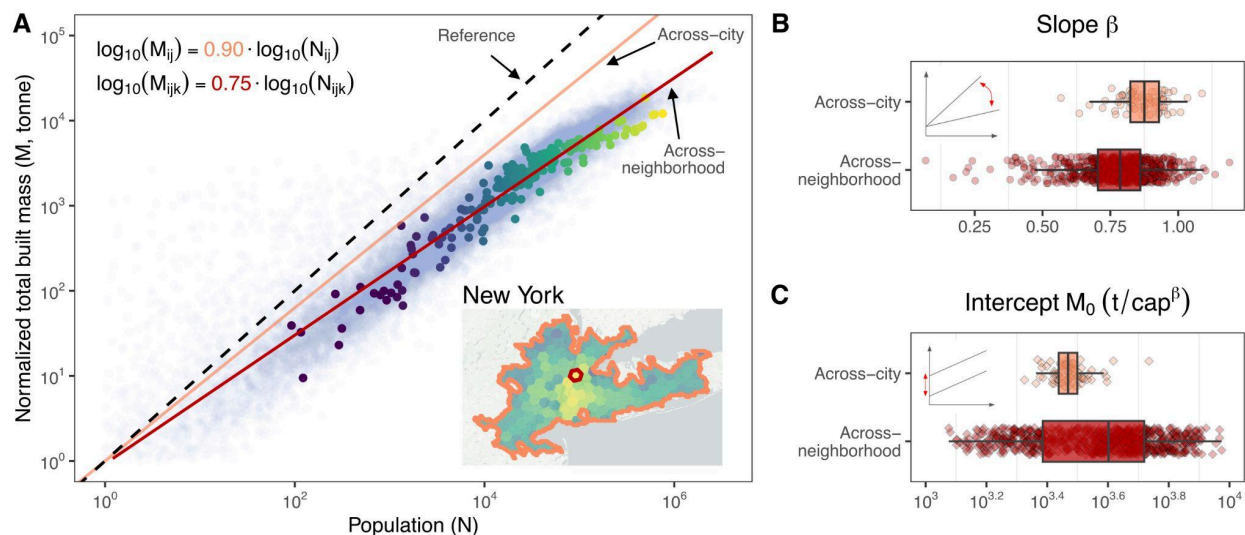


Figure 3| Sublinear scaling of built mass across neighborhoods. (A) Log-log scatter plot of the normalized total built mass M (in tonnes) versus population N for the k -th neighborhood (in the j -th city and the i -th country), with regression lines showing the across-neighborhood scaling relationship (red, slope $\delta = 0.75$; $n=34,045$; $R^2=0.85$) and the across-city relationship (orange, slope $\beta = 0.9$). The dashed

black line indicates linear scaling (slope = 1). Colored points highlight neighborhoods in New York, with an inset hex map showing their spatial distribution of population. Boxplots of the fitted slopes (**B**) and intercepts (**C**) from these regressions compare the distributions of across-city fits within countries (orange) and across-neighborhood fits within cities (red), showing larger variations in the across-neighborhood regressions.

Economies of scale at the neighborhood level

Across a global dataset of urban neighborhoods, we observe that built material mass increases sublinearly with population in both across-city and across-neighborhood comparisons. Importantly, because each neighborhood polygon in our sample has nearly the same land area, its “population” can be considered a measure of density—unlike whole-city population size, which combines density and total area. Using a multilevel fixed-effects model (see Methods), with separate intercepts by city and country but a common slope, we estimate a markedly lower scaling exponent within cities ($\delta = 0.75$; red line in Fig.3A) than across entire cities ($\beta = 0.90$; orange line).

Each neighborhood sits within a single city, and each city within a country, so this nested structure captures local “baselines” for building mass while isolating the universal sublinear trend. The result implies that as local density increases (i.e., more people per fixed area), the extra built mass needed per additional resident falls off more steeply than when comparing cities of different sizes and footprints. Figure 3 compares fitted slopes (panel B) and intercepts (panel C) at two scales—neighborhoods within cities (red) and cities within countries (orange)—and shows that finer-scale fits vary more. The distribution of neighborhood-level slopes is both broader and shifted to lower values, and the intercepts span a wider range, reflecting strong local heterogeneity in land-use intensity and infrastructure clustering. In other words, local density effects within a city generate even more pronounced economies of scale than aggregate city-to-city comparisons.

Our findings expand upon and unify several strands of recent research. Prior studies (16, 24) have found lower per capita mobility infrastructure mass in denser urban areas. Other research (15, 32) similarly indicates that total built mass per capita is lower in denser urban settings but without systematically quantifying these relationships. Sublinear scaling patterns for building volumes have been identified within 10 individual Chinese cities (33), but this study is geographically limited, raising the question of global generalizability.

Our analysis addresses this gap by demonstrating a universal sublinear scaling trend in total built mass at the neighborhood level across thousands of cities worldwide. Moreover, by explicitly contrasting within-city and across-city patterns, we show that stronger economies of scale emerge at finer spatial resolutions—underscoring the importance of multi-scalar analysis in urban metabolism research. This raises a key theoretical question: why does the scaling exponent increase when moving from local ($\delta = 0.75$) to aggregate scales ($\beta = 0.9$), and what mechanisms can bridge these levels?

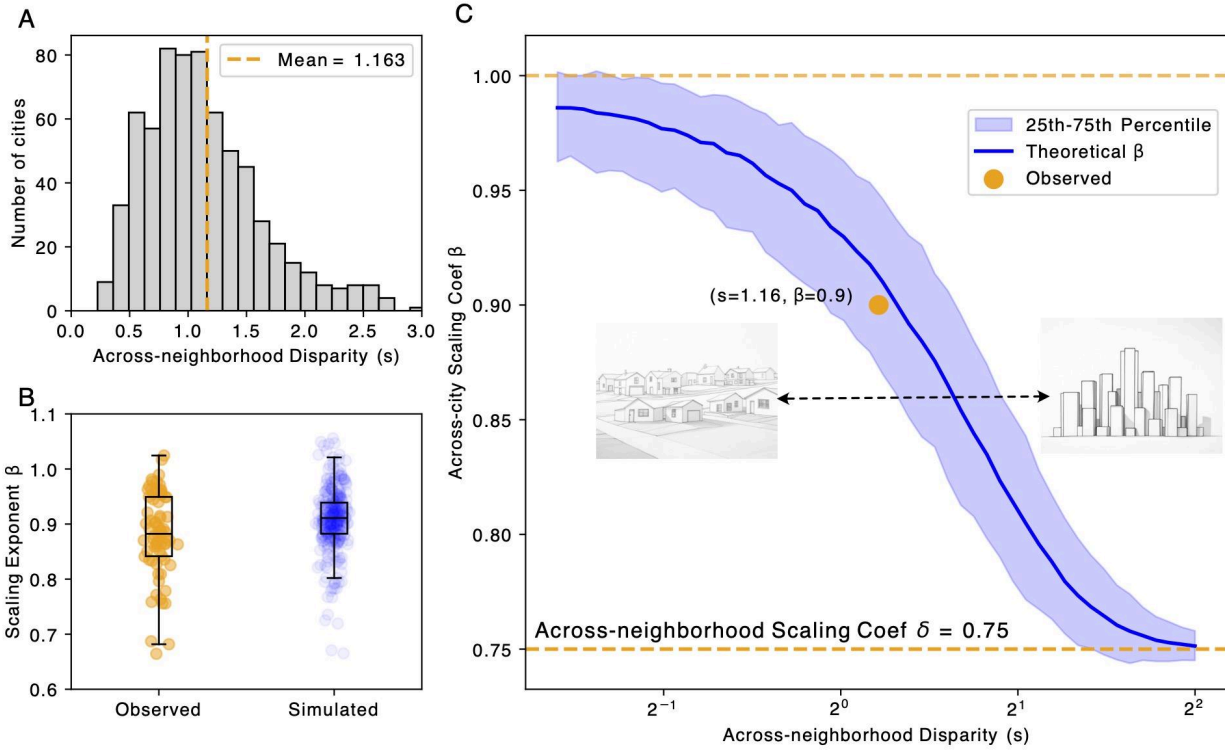


Figure 4| Emergence of sublinear across-city scaling from across-neighborhood disparity. The disparity parameter s (Zipf’s exponent) captures how uneven population is distributed across neighborhoods—larger s indicates greater disparity (a few dense neighborhoods dominate), while smaller s reflects more uniform distributions. (A) Probability distribution of s across cities, with the mean ($s = 1.16$) marked by a dashed line. (B) Boxplots comparing observed city-level scaling exponents β (orange) with those predicted by theoretical simulations (blue), showing strong agreement. Simulated cities assume Zipf-like neighborhood population distributions and a fixed within-city scaling exponent ($\delta=0.75$). In each box plot, the lower and upper bounds of the whiskers denote minima and maxima, the center line denotes the median, and the lower and upper bounds of the boxes represent the 25% and 75% quantiles, respectively. (C) Theoretical relationship between s and β (solid blue line): a system of more homogenous cities (illustration showing cities with uniform single family housing districts, small s) approaches linear scaling (upper bound, $\beta \approx 1$), while a system of more heterogeneous cities (illustration showing cities with buildings of varying heights, large s) converges toward the within-city exponent (lower bound, $\delta=0.75$). The empirical means ($s=1.16, \beta=0.90$, orange point) aligns with this trend.

Emergence of across-city sublinear scaling from across-neighborhood disparity

We hypothesize that the degree of population heterogeneity is the key that bridges scaling across the two nested spatial scales: across cities ($\beta = 0.90$) and across neighborhoods ($\delta = 0.75$). Existing research suggests that neighborhood populations often conform to Zipf-like, heavy-tailed distributions, where a small number of dense neighborhoods house disproportionately larger amounts of residents (17, 34, 35). Given the sublinear scaling of built mass at the neighborhood level, these dense areas benefit from enhanced economies of scale, reducing the per capita built mass at the city-wide level.

To test this hypothesis, we developed a theoretical model comprising simulated cities with neighborhoods whose populations follow a Zipf-like distribution governed by an across-neighborhood disparity parameter s (see Methods). Neighborhood-level built mass was assigned using the empirical scaling exponent ($\delta = 0.75$), then aggregated to obtain total city-level built mass (M) and population (N). We estimated the across-city scaling exponent β by regressing $\log(M)$ against $\log(N)$ across these simulated

cities. We introduced two random processes to capture the variability: 1) we drew a random s parameter from a normal distribution, centered at the given s with a standard deviation (0.59) estimated from the observed distribution (Fig.4A); 2) we grouped the cities randomly into “countries” and conducted separate regressions, producing a distribution of theoretical β values.

We found that the observed distribution of disparity parameter s is right-skewed (Fig.4A), which suggests that many cities have very heterogeneous neighborhoods (*i.e.*, coexistence of very dense and very sparse neighborhoods). Based on the observed distribution of s (mean=1.16, std=0.59), we simulated across-city scaling exponents (β), which strongly aligns with observed exponents (Fig.4B). By sweeping various values of s , our simulations further elucidate the theoretical relationship between neighborhood disparity s and city-level scaling exponent β , depicting a smoothly declining curve from nearly linear ($\beta \approx 1.0$) at low disparity to strongly sublinear (β approaching $\delta = 0.75$) at high disparity (Fig.4C). Our mathematical derivation (SI Methods) further illustrates that across-city scaling exponent β is intrinsically bounded by two limits ($\delta \leq \beta \leq 1$), explaining the increase of exponent when moving from local (neighborhood) to the aggregate (city).

Our empirical analysis and theoretical simulations indicate that within-city density disparities are a critical mechanism underpinning economies of scale in built material use. Denser neighborhoods—often housing a disproportionate share of the urban population—require less built mass per capita, thereby driving the sublinear scaling observed at the city level. Classical urban economic models (36–38) provide a well-established explanation for the emergence of these disparities. In monocentric cities, proximity to the central business district raises land values and incentivizes denser development near the core. In polycentric cities, multiple subcenters generate additional peaks of accessibility and land value, sustaining density gradients as households and firms cluster around these nodes (39).

However, zoning regulations and density constraints can suppress this natural tendency toward concentrated development (40). Restrictions such as maximum floor-area ratios, height limits, or exclusionary zoning limit high-density construction in areas with strong market demand, effectively flattening the urban density gradient (decreasing s and increasing β) (41). As a result, such anti-density interventions may unintentionally nullify the material efficiency gains associated with urban density variation—undermining the very mechanism that enables cities to use built materials more efficiently.

Managing cities as nested complex systems

Our analysis indicates that conventional per-capita projections systematically overestimate the required built mass in larger cities and denser neighborhoods. According to the latest IPCC assessment report(42, 43), cement and steel—critical materials primarily used for built mass—account for ~5.2 GtCO₂-eq/yr of global emissions. From 2018 to 2050, the cumulative buildings, infrastructure and machinery-related emissions are projected (11) to reach between 1,300 and 2,100 GtCO₂-eq, driven mainly by increasing material stocks. Yet these projections treat every future urban resident as if they would require the same amount of material irrespective of the size or form of the city they live in.

Neglecting size-dependent nonlinear scaling can lead to substantial mis-estimations in material demand—an issue made clear when re-examining a recent UN-Habitat projection(44) through the lens of our findings. This projection shows that, in low-income countries, the population living in megacities ($N > 5$ millions) will rise from 18 million today to about 140 million by 2070. In those countries, the projected future population living in megacities will be roughly equal to the population (~160M) that now inhabit small cities ($N < 250k$). Under the across-city scaling relationship revealed here ($\beta = 0.9$), multiplying city population size by twenty ($250k \rightarrow 5M$) raises per-capita material demand by only $20^\beta \approx 14.8$, not twenty-fold. This means that accommodating the same number of people in megacities, instead of small cities, reduces the per-capita material footprint by roughly 26% ($1 - 14.8/20 \approx 0.26$). Therefore, policies that cap city size could erase an important material-efficiency gain.

Within cities we find a steeper sub-linear scaling of built mass with population density ($\delta = 0.75$, by definition “per-capita” scaling coefficient is $0.75 - 1 = -0.25$). Unfortunately, existing scenario studies(44, 45) stop at country-level averages and cannot tell us how many people will live in very-high- or very-low-density neighborhoods. For example, in one potential scenario, UN-Habitat projections(44) suggest that average urban density in low-income countries could increase to 164% of current levels by 2050. If this happens, and we apply our scaling exponent ($\delta = 0.75$), the per-capita built mass in a neighborhood would decrease by 12% ($1.64^{-0.25}=0.88$) compared to linear projections. However, this average-density scenario still overlooks the heterogenous non-linear effects across various neighborhoods. Therefore, future projections must shift from average densities to distributions among multiple density-levels if we are to understand the real material stakes of urban growth.

Beyond material efficiency, urban scale and density also lead to significant socioeconomic advantage. Large cities enable deeper labor market pooling, specialized supplier networks, and extensive knowledge-sharing, all of which bolster innovation and productivity(46). For instance, a bigger urban population allows a finer division of labor and supports niche industries and services that require a broad customer base, which tend to cluster in major cities(47). High population density further reduces the spatial separation between people and opportunities, facilitating efficient matching in the labor market and easy access to specialized services(48). Dense neighborhoods also foster more frequent face-to-face interactions and serendipitous encounters—the “unplanned synergies” that Jacobs (1961)(49) noted in large cities—which can spark innovation and connect individuals with rare skills or interests. In fact, even a tiny fraction of people with a niche interest can form a critical mass in a metropolis(50). Together, these mechanisms suggest that urban scale and density are key drivers of social and economic opportunities, providing access to spatialized markets, services, and social networks that less dense or smaller urban areas cannot easily support.

While increasing city sizes and neighborhood densities can enhance material efficiency and bring socioeconomic advantages, unchecked growth and densification can intensify social and public health challenges. For instance, larger cities often experience disproportionate increases in congestion, crime, infectious diseases, as these outcomes scale superlinearly with population size, reflecting the complex dynamics of urban environments (51–53). Moreover, in densely populated urban slums, shared sanitation facilities are prevalent due to limited space and resources, but poor maintenance and hygiene often lead to health risks and diminished quality of life (54). The collective responsibility for maintaining such facilities frequently results in neglect, as individuals are less motivated to care for shared spaces. These challenges highlight the need to balance material efficiency with investments in infrastructure that ensure adequate living standards (55) and public health in high-density urban areas.

Taken together, our findings collectively underscore the importance to recognize these linked, multi-scale material efficiencies as intrinsic properties of cities. Viewing cities as complex adaptive systems—whose performance depends jointly on their overall size and their hierarchically nested internal structure(56, 57) will enable more holistic and effective policy interventions in the pursuit of a more productive, equitable, and sustainable urban future.

Statistical analyses**Data availability**

Data will be made available on public online depository (figshare) upon publication.

Code availability

Code will be made available on public online depository (figshare) upon publication.

Acknowledgement

This work was supported by a New York University internal grant awarded to M.L. and K.H. We thank Aiyu Zheng, Jacob Levine, Ignacio Arroyo, Karen Seto, members of Seto lab and colleagues at Department of Environmental Studies for helpful comments on the manuscript.

Author Contribution

K.H. and M.L. developed the overall conceptual framework, carried out analysis, designed visualization, wrote the paper together. Both authors contributed equally.

Competing Interests Statement

The authors declare no competing interests.

Reference

1. Z. Ao, X. Hu, S. Tao, X. Hu, G. Wang, M. Li, F. Wang, L. Hu, X. Liang, J. Xiao, A. Yusup, W. Qi, Q. Ran, J. Fang, J. Chang, Z. Zeng, Y. Fu, B. Xue, P. Wang, K. Zhao, L. Li, W. Li, Y. Li, M. Jiang, Y. Yang, H. Shen, X. Zhao, Y. Shi, B. Wu, Z. Yan, M. Wang, Y. Su, T. Hu, Q. Ma, H. Bai, L. Wang, Z. Yang, Y. Feng, D. Zhang, E. Huang, J. Pan, H. Ye, C. Yang, Y. Qin, C. He, Y. Guo, K. Cheng, Y. Ren, H. Yang, C. Zheng, J. Zhu, S. Wang, C. Ji, B. Zhu, H. Liu, Z. Tang, Z. Wang, S. Zhao, Y. Tang, H. Xing, Q. Guo, Y. Liu, J. Fang, A national-scale assessment of land subsidence in China's major cities. *Science* **384**, 301–306 (2024).
2. G. Chure, R. A. Banks, A. I. Flamholz, N. S. Sarai, M. Kamb, I. Lopez-Gomez, Y. M. Bar-On, R. Milo, R. Phillips, The Anthropocene by the Numbers: A Quantitative Snapshot of Humanity's Influence on the Planet, *arXiv [physics.soc-ph]* (2021). <http://arxiv.org/abs/2101.09620>.
3. E. Elhacham, L. Ben-Uri, J. Grozovski, Y. M. Bar-On, R. Milo, Global human-made mass exceeds all living biomass. *Nature* **588**, 442–444 (2020).
4. C. Morgan, D. Webb, K. Sprengeler, M. (pedro) Black, N. George, Experimental construction of hunter-gatherer residential features, mobility, and the costs of occupying “persistent places.” *J. Archaeol. Sci.* **91**, 65–76 (2018).
5. E. C. Stokes, K. C. Seto, Characterizing and measuring urban landscapes for sustainability. *Environ. Res. Lett.* **14**, 045002 (2019).
6. A. Cattaneo, S. Girgin, R. de By, T. McMenomy, A. Nelson, S. Vaz, Worldwide delineation of multi-tier city–regions. *Nat Cities* **1**, 469–479 (2024).
7. S. A. Spawn, C. C. Sullivan, T. J. Lark, H. K. Gibbs, Harmonized global maps of above and belowground biomass carbon density in the year 2010. *Sci. Data* **7**, 112 (2020).
8. F. Krausmann, C. Lauk, W. Haas, D. Wiedenhofer, From resource extraction to outflows of wastes and emissions: The socioeconomic metabolism of the global economy, 1900–2015. *Glob. Environ. Change* **52**, 131–140 (2018).
9. United Nations Publications, *World Urbanization Prospects: The 2018 Revision* (UN, 2019).
10. M. Hajer, M. Baynes, T. Bergesen, J. Labbé, F. Musango, J. K. Ramaswami, A. Robinson, B. Salat, S. Suh, S. Currie, P. Fang, A. Hanson, A. Kruit, K. Reiner, M. Smit, S. Tabory, “The Weight of Cities: Resource Requirements of Future Urbanization. Swilling” (Nairobi, Kenya, 2018).
11. F. Krausmann, D. Wiedenhofer, H. Haberl, Growing stocks of buildings, infrastructures and machinery as key challenge for compliance with climate targets. *Glob. Environ. Change* **61**, 102034 (2020).
12. L. M. A. Bettencourt, The origins of scaling in cities. *Science* **340**, 1438–1441 (2013).
13. L. M. A. Bettencourt, Urban growth and the emergent statistics of cities. *Sci Adv* **6**, eaat8812 (2020).
14. M. Lu, C. Zhou, C. Wang, R. B. Jackson, C. P. Kempes, Worldwide scaling of waste generation in urban systems. *Nat Cities* **1**, 126–135 (2024).
15. D. Frantz, F. Schug, D. Wiedenhofer, A. Baumgart, D. Virág, S. Cooper, C. Gómez-Medina, F. Lehmann, T. Udelhoven, S. van der Linden, P. Hostert, H. Haberl, Unveiling patterns in human

- dominated landscapes through mapping the mass of US built structures. *Nat. Commun.* **14**, 8014 (2023).
16. D. Wiedenhofer, A. Baumgart, S. Matej, D. Virág, G. Kalt, M. Lanau, D. D. Tingley, Z. Liu, J. Guo, H. Tanikawa, H. Haberl, Mapping and modelling global mobility infrastructure stocks, material flows and their embodied greenhouse gas emissions. *J. Clean. Prod.* **434**, 139742 (2024).
 17. T. Louail, M. Lenormand, O. G. Cantu Ros, M. Picornell, R. Herranz, E. Frias-Martinez, J. J. Ramasco, M. Barthelemy, From mobile phone data to the spatial structure of cities. *Sci. Rep.* **4**, 5276 (2014).
 18. M. Li, Y. Wang, J. F. Rosier, P. H. Verburg, J. van Vliet, Global maps of 3D built-up patterns for urban morphological analysis. *Int. J. Appl. Earth Obs. Geoinf.* **114**, 103048 (2022).
 19. X. Liu, X. Wu, X. Li, X. Xu, W. Liao, L. Jiao, Z. Zeng, G. Chen, X. Li, Global mapping of three-dimensional (3D) urban structures reveals escalating utilization in the vertical dimension and pronounced building space inequality. *Engineering (Beijing)*, doi: 10.1016/j.eng.2024.01.025 (2024).
 20. T. Esch, E. Brzoska, S. Dech, B. Leutner, D. Palacios-Lopez, A. Metz-Marconcini, M. Marconcini, A. Roth, J. Zeidler, World Settlement Footprint 3D - A first three-dimensional survey of the global building stock. *Remote Sens. Environ.* **270**, 112877 (2022).
 21. J. R. Meijer, M. A. J. Huijbregts, K. C. G. J. Schotten, A. M. Schipper, Global patterns of current and future road infrastructure. *Environ. Res. Lett.* **13**, 064006 (2018).
 22. X. Huang, J. Yang, W. Wang, Z. Liu, Mapping 10-m global impervious surface area (GISA-10m) using multi-source geospatial data (2022). <https://doi.org/10.5194/essd-2021-458>.
 23. M. Melchiorri, M. Pesaresi, A. J. Florczyk, C. Corbane, T. Kemper, Principles and applications of the Global Human Settlement Layer as baseline for the Land Use Efficiency indicator—SDG 11.3.1. *ISPRS Int. J. Geoinf.* **8**, 96 (2019).
 24. L. S. A. Rousseau, B. Klooststra, H. AzariJafari, S. Saxe, J. Gregory, E. G. Hertwich, Material stock and embodied greenhouse gas emissions of global and urban road pavement. *Environ. Sci. Technol.* **56**, 18050–18059 (2022).
 25. H. Haberl, A. Baumgart, J. Zeidler, F. Schug, D. Frantz, D. Palacios-Lopez, T. Fishman, Y. Peled, B. Cai, D. Virág, P. Hostert, D. Wiedenhofer, T. Esch, Weighing the global built environment: High-resolution mapping and quantification of material stocks in buildings. *J. Ind. Ecol.* **29**, 159–172 (2025).
 26. A. Marshall, *Principles of Economics* (Springer, 2013).
 27. S. S. Rosenthal, W. C. Strange, “Chapter 49 Evidence on the nature and sources of agglomeration economies” in *Handbook of Regional and Urban Economics* (Elsevier, 2004)vol. 4 of *Handbook of regional and urban economics*, pp. 2119–2171.
 28. L. M. A. Bettencourt, J. Lobo, D. Helbing, C. Kühnert, G. B. West, Growth, innovation, scaling, and the pace of life in cities. *Proc. Natl. Acad. Sci. U. S. A.* **104**, 7301–7306 (2007).
 29. F. L. Ribeiro, D. Rybski, Mathematical models to explain the origin of urban scaling laws. *Phys. Rep.* **1012**, 1–39 (2023).

30. Z. Xu, G. Xu, T. Lan, X. Li, Z. Chen, H. Cui, Z. Zhou, H. Wang, L. Jiao, C. Small, Global consistency of urban scaling evidenced by remote sensing. *PNAS Nexus* **4**, gaf037 (2025).
31. K. Yakubo, Y. Saijo, D. Korošak, Superlinear and sublinear urban scaling in geographical networks modeling cities. *Phys. Rev. E Stat. Nonlin. Soft Matter Phys.* **90**, 022803 (2014).
32. W. Mikhelson, H. Arbabi, S. Hincks, D. D. Tingley, Built-environment stocks in the context of a master-planned city: A case study of Chandigarh, India. *J. Ind. Ecol.* **28**, 573–588 (2024).
33. L. Dong, Z. Huang, J. Zhang, Y. Liu, Understanding the mesoscopic scaling patterns within cities. *Sci. Rep.* **10**, 21201 (2020).
34. J. Li, D. Wong, D. A. Griffith, Exploring and simulating the regularities in intra-urban population density structure. *Ann. GIS* **15**, 11–22 (2009).
35. R. Lemoy, G. Caruso, Evidence for the homothetic scaling of urban forms. *Environ. Plan. B Urban Anal. City Sci.* **47**, 870–888 (2020).
36. W. Alonso, *Location and Land Use: Toward a General Theory of Land Rent* (Harvard University Press, Cambridge, MA, 1964).
37. E. S. Mills, An Aggregative Model of Resource Allocation in a Metropolitan Area. *American Economic Review* **57**, 197–210 (1967).
38. R. F. Muth, *Cities and Housing: The Spatial Pattern of Urban Residential Land Use* (University of Chicago Press, Chicago, 1969).
39. C. Liotta, V. Vigiú, Q. Lepetit, Testing the monocentric standard urban model in a global sample of cities. *Reg. Sci. Urban Econ.* **97**, 103832 (2022).
40. J. Gyourko, R. Molloy, “Regulation and housing supply” in *Handbook of Regional and Urban Economics* (Elsevier, 2015) vol. 5 of *Handbook of regional and urban economics*, pp. 1289–1337.
41. J. T. Rothwell, D. S. Massey, Density zoning and class segregation in U.S. metropolitan areas: Density zoning and class segregation. *Soc. Sci. Q.* **91**, 1123–1143 (2010).
42. I. A. Bashmakov, L. J. Nilsson, A. Acquaye, C. Bataille, J. M. Cullen, S. de la R. du Can, M. Fischedick, Y. Geng, K. Tanaka, “Industry” in *Climate Change 2022: Mitigation of Climate Change. Contribution of Working Group III to the Sixth Assessment Report of the Intergovernmental Panel on Climate Change*, P. R. Shukla, J. Skea, R. Slade, A. A. Khourdajie, R. van Diemen, D. McCollum, M. Pathak, S. Some, P. Vyas, R. Fradera, M. Belkacemi, A. Hasija, G. Lisboa, S. Luz, J. Malley, Eds. (Cambridge University Press, Cambridge, UK and New York, NY, USA, 2022).
43. L. F. Cabeza, Q. Bai, P. Bertoldi, J. M. Kihila, A. F. P. Lucena, É. Mata, S. Mirasgedis, A. Novikova, Y. Saheb, “Buildings” in *Climate Change 2022: Mitigation of Climate Change. Contribution of Working Group III to the Sixth Assessment Report of the Intergovernmental Panel on Climate Change*, P. R. Shukla, J. Skea, R. Slade, A. A. Khourdajie, R. van Diemen, D. McCollum, M. Pathak, S. Some, P. Vyas, R. Fradera, M. Belkacemi, A. Hasija, G. Lisboa, S. Luz, J. Malley, Eds. (Cambridge University Press, Cambridge, UK and New York, NY, USA, 2022).
44. World cities report 2022 : envisaging the future of cities. xxxi, 387 p. : (2022).
45. B. Güneralp, Y. Zhou, D. Ürge-Vorsatz, M. Gupta, S. Yu, P. L. Patel, M. Fragkias, X. Li, K. C. Seto,

- Global scenarios of urban density and its impacts on building energy use through 2050. *Proc. Natl. Acad. Sci. U. S. A.* **114**, 8945–8950 (2017).
46. G. Giuliano, S. Kang, Q. Yuan, Agglomeration economies and evolving urban form. *Ann. Reg. Sci.* **63**, 377–398 (2019).
 47. H. R. A. Koster, J.-F. Thisse, Understanding spatial agglomeration: Increasing returns, land, and transportation costs. *Annu. Rev. Econom.* **16**, 55–78 (2024).
 48. S. S. Rosenthal, W. C. Strange, How close is close? The spatial reach of agglomeration economies. *J. Econ. Perspect.* **34**, 27–49 (2020).
 49. J. Jacobs, *The Death and Life of Great American Cities* (Random House, New York, NY, 1961) *Pelican books*.
 50. C. S. Fischer, Toward a Subcultural Theory of Urbanism. *Am. J. Sociol.* **80**, 1319–1341 (1975).
 51. E. M. McCulley, P. H. Mullachery, A. F. Ortigoza, D. A. Rodríguez, A. V. Diez Roux, U. Bilal, Urban scaling of health outcomes: A scoping review. *J. Urban Health* **99**, 409–426 (2022).
 52. L. M. A. Bettencourt, J. Lobo, D. Strumsky, G. B. West, Urban scaling and its deviations: revealing the structure of wealth, innovation and crime across cities. *PLoS One* **5**, e13541 (2010).
 53. R. Louf, M. Barthelemy, How congestion shapes cities: from mobility patterns to scaling. *Sci. Rep.* **4** (2014).
 54. J. B. Tidwell, J. Chipungu, I. Ross, P. Antwi-Agyei, M.-U. Alam, I. K. Tumwebaze, G. Norman, O. Cumming, S. Simiyu, Where shared sanitation is the only immediate option: A research agenda for shared sanitation in densely populated low-income urban settings. *Am. J. Trop. Med. Hyg.* **104**, 429–432 (2020).
 55. J. A. Vélez-Henao, S. Pauliuk, Material requirements of decent living standards. *Environ. Sci. Technol.* **57**, 14206–14217 (2023).
 56. M. Batty, The size, scale, and shape of cities. *Science* **319**, 769–771 (2008).
 57. M. Barthelemy, The statistical physics of cities. *Nat. Rev. Phys.* **1**, 406–415 (2019).

Nested economies of scale in city mass

Kangning Huang, Mingzhen Lu

Table of contents

- 1. Materials and Methods**
- 2. Figures**
- 3. Tables**
- 4. References**

Materials and methods

Historical trend of global built structure mass

We derived historical global population data from our world in data (<https://ourworldindata.org/grapher/population>). We acquired the global built structure mass and global biomass dataset from Elhacham et al. (2020) from 1900 to 2015 and projection data from 2015 to 2037(1). We used linear interpolation (`zoo::na.approx()`) to interpolate missing global biomass value during 1991-1999, 2001-2009, 2011, 2013-2016. To calculate the built structure to human mass ratio, we estimated weighted average human body mass as approximately 50 kg. We derived this coarse-grained estimation by combining the global average age distribution (25% 0-14, 65% 15-64, 10% 65+ in year 2023 based on World Bank data, <https://data.worldbank.org/indicator/SP.POP.0014.TO.ZS>) with the age-specific body mass (25kg for 0-14, 60kg for 15-64, 50kg for 65+). We are aware that age-specific body mass varies across countries, regions, diets, and a range of other factors, however, the qualitative conclusions presented in our work are not sensitive to the uncertainties associated with this estimation.

Vegetation biomass

We extracted city-specific vegetation biomass from a recently published global map of vegetation carbon that includes both aboveground and belowground biomass carbon (2). The vegetation carbon data is based on 2010. We then converted biomass carbon into dry-weight vegetation biomass using a convection coefficient of 0.48g carbon per gram of dry-weight biomass (3). We extracted city-specific vegetation biomass based on city definitions described in the following section.

Definition of cities

In this study, we define cities using the concept of Urban Cores (UC) provided by the Global Human Settlement Layer (GHSL). GHSL, developed by the European Commission's Joint Research Centre, delineates urban cores based on continuous areas of built-up land and population density, derived from satellite imagery and census data(4). An urban core is typically characterized by contiguous built-up surfaces with high population density, representing the primary agglomeration of urban activity within a region. Following established conventions, we include only cities with a minimum population size of 50,000 residents in our analysis, ensuring consistency and comparability with other global urban studies (5, 6). This operational definition allows us to systematically evaluate and compare urban built environments and associated resource demands across a diverse range of global cities. Our main finding that economies of scale in urban built stock is prevalent in cities worldwide is robust to the arbitrary cutoff sizes of cities. In fact, we would argue that the exact cutoff of city definition is not so important given the self-similarity, or fractal-like feature of urban built stock.

Definition of neighborhoods

We delineate neighborhoods with the H3 global hexagonal grid (developed by Uber)(7). Hexagons have two properties that are critical for our analysis. First, among the few regular polygons that tessellate the plane, hexagons minimize the perimeter-to-area ratio, yielding compact, near-circular units that reduce edge effects when we aggregate spatial data. Second, hexagons tile space without the directional bias that characterizes squares (Manhattan effect) or triangles, thereby supporting isotropic distance measures that better approximate real-world movement patterns. These features mirror the intuition of Christaller's central-place theory(8), which idealizes market areas as hexagons to maximize coverage while minimizing overlap. Here we use the hexagons at resolution of level-6, where each cell has an average edge length of ~3.7 km and an area of 37 km², a scale that captures the extent of day-to-day human activity: the cell radius can be covered in ~15 min by bicycle (15 km/h) or ~45 min on foot (5 km/h). The resulting neighborhoods are therefore large enough to encompass the functional mix of a self-contained urban district, yet fine-grained enough to retain intra-city variation in the variables we study.

Bottom-up approach of urban built stock

To quantify the material stocks embedded in the built environment of cities, we devised a workflow that is the first global analysis that builds up the total mass of urban buildings and paved surfaces from the ground up. This method separately estimates the volumes of building and areas of mobility infrastructure within each city boundary and relies on well-established, type-specific and region-specific material intensity factors to convert built volume, road surface, and pavements into mass, detailed below.

1) Stock of buildings. We use raster-based estimates of building volume provided independently by Esch et al. (2022)(9), Li et al. (2022)(10), and Liu et al. (2024)(11), which offer 3D characterizations of urban form at various spatial resolutions. To minimize dataset-specific bias, we calculate the average building volume within each city boundary using all three datasets.

Table S1| Summaries of input 3D building datasets

Source	Input Imagery (years)	Resolution	RMSE (volume)
Esch et al. (2022)	TanDEM-X amplitude (2011, 2013); WSF 2019 mask (Sentinel-1/2 pre-2019);	90 m	1.54 m ³ /m ²
Li et al. (2022)	Landsat-8 (2015); Sentinel-1 (2015–2016);	1 km	0.619 m ³ /m ²
Liu et al. (2024)	Sentinel-1 (2015); ALOS (2015); Landsat-8 (2014-2016);	500 m	0.243 m ³ /m ²

We then converted building volume to built stock mass using a detailed material intensity framework that considers both (1) building types and (2) regional construction practices developed by Haberl et al. (2025) for analyzing global buildings (12). We distinguish building types based on GHS-BUILT-S classifications, as the distinct function and form of different building types demands different building standards and consequently different material intensities independent of country and region. Similarly, material intensity is also a function of country and region due to the dependence of building on local climate, building practices, developmental level, etc. In Table.S1 we provide a summary look-up table for matching building types to material intensities. For the detailed regional breakdown (OECD, North America, Japan, China, etc.), please refer to Haberl et al. (2025) Table.S5.

Table.S2 Material intensity as a function of building type and region.

Building type	Building height (m)	GHS-BUILT-S (class)	Region-specific material intensity (kg/m ³)
Lightweight (LW)	< 3	Residential + non-residential	151–154
Residential single-family house (RS)	3–12	Residential	125–526
Residential multi-family house (RM)	12–50	Residential	315–662
Non-residential (NR)	3–50	Non-residential	273–654
High-rise (HR)	50–100	Residential + non-residential	312–330

2) Stock of mobility infrastructure and other pavement. For impervious surface data, we use the GISA-10m product from Huang et al. (2022)(13), which maps global impervious cover at 10-meter resolution. To isolate the portion of impervious surface attributable to pavement (e.g., roads, sidewalks), we subtract the building footprint area—estimated from the previous step by averaging Li et al. (2022)(10), Liu et al. (2024)(11) and Esch et al. (2022)(9)—from the total impervious surface within each city.

After extracting pavement area, we further tease out 5 grades of roads network vs. other pavements (sidewalks, parking lot) given the big difference in their required structural intensity and consequently material intensity. For each city, we calculate the total length and total area of the road network per road grade: with decreasing material intensity, highway, primary, secondary, tertiary, and local. We then convert road area to road stock mass based on a type-specific and region-specific material intensity lookup table (summarised in Table. S2, full table uploaded as separate file, derived from (14))

Road Type	# Lanes (approx.)	Lane width (per lane, m)	Region- and climate-specific material intensity (kg/m ²)
Highway	3 – 7	3.0 – 4.0	910.6 – 2883.5
Primary	2 – 5	3.0 – 4.0	803.9 – 2331.5
Secondary	1 – 5	2.4 – 4.1	768.1 – 1817.9
Tertiary	1 – 4	2.4 – 4.1	647.7 – 1750.8
Local	1 – 3	2.4 – 4.1	538.5 – 1548.2

For other pavements (e.g., sidewalks, parking lot), we assume a material intensity of 570 kg/m² (equivalent to about 20 cm of concrete or asphalt), a value lower than typical road material intensity adopted by previous meta-analysis in the field of industrial ecology (see Frantz et al. 2023 Table.S15 for parking lots (15)).

The total mass of urban built stock is the sum of the estimated building, road mass and other pavement mass. This bottom-up approach provides a consistent and scalable method to compare material stocks across global cities using spatially explicit data.

Data acquisition for urban population

We used the WorldPop dataset to calculate the total population of each city by summing pixels within city boundaries from WorldPop raster datasets. We chose WorldPop due to its high spatial resolution (100m), detailed demographic representation, frequent updates, and open accessibility, providing reliable population data that better captures population distributions compared to other gridded population datasets(16, 17). WorldPop integrates diverse data sources, including satellite imagery, census, and ancillary data, making it particularly suitable for accurately mapping populations within urban areas.

Scaling theory and fixed slope analysis

Scaling theory studies the change of system properties as a system changes in its size (18). Its conceptual foundation can at least be traced back to early insight regarding proportional scaling up (*i.e.*, linear scaling) built infrastructure in Galileo's *Two New Sciences* (19). Galileo deduced that scaling structures proportionally in size increases their volume and mass at a faster rate than the increase of strength, leading to structural failures. Mathematically, this type of relationship is expressed through power-law equations of the general form:

$$Y = Y_0 N^\beta$$

In this equation, Y denotes a measurable property or characteristic of the system, N represents system size, β is the scaling exponent capturing how quickly a property changes relative to system size, and Y_0 is the normalization constant, representing the elevation of the scaling relationship on a log-log plot (20, 21), providing insights into the baseline or developmental level of the system (*e.g.*, a collection of buildings, a taxon of multiple species, or a group of cities).

Aside from its widespread application in physics and engineering, scaling theory significantly influenced biology through the early 20th-century subfield of allometric analysis, enhancing the adoption and interpretation of Darwin's evolutionary theory (22–25). Notable examples include scaling relationships such as organism body mass with metabolic rate and tree height with stem diameter. These foundational biological concepts were further expanded by West, Brown, and Enquist, who formalized biological scaling laws, laying the groundwork for applications in other complex systems, including urban contexts initiated by Bettencourt and colleagues (26).

Scaling theory has recently been widely adopted to enhance our understanding of urban systems, elucidating how a wide range of urban indicators (wealth, innovation, crime, infrastructure, waste, etc.) scale with city population size (6, 27). Variations in the exponent indicate critical nonlinearities—economies or diseconomies of scale—that are often obscured by simple per-capita measures. Superlinear scaling ($\beta > 1$) characterizes intensified social interactions and innovation typically seen in larger cities, whereas sublinear scaling ($\beta < 1$) describes constraints related to physical infrastructure and spatial limits (28).

To statistically manage correlations between the scaling exponent β and normalization constant Y_0 , the method of fixing slope and estimating elevation is commonly applied, originating from biological analyses(20, 29, 30). We use this statistical approach to derive nation-specific baselines in cross-city analyses and city-specific baselines at neighborhood scales, allowing us to normalize data effectively and focus explicitly on scaling slopes to reveal fundamental urban dynamics.

Multi-level Fixed-effect Scaling Analysis

In our multi-level fixed-effect scaling model, we regress the logarithm of built mass M_{ijk} in neighborhood k of city j in country i on the logarithm of neighborhood population N_{ijk} , while absorbing separate intercepts for each country and each city. In compact form, the model is

$$\log(M_{ijk}) = \gamma_0 + \gamma_i + \gamma_j + \delta \cdot \log(N_{ijk}) + \varepsilon_{ijk}$$

where γ_0 is the global baseline intercept, γ_i the deviation for country i , and γ_j the deviation for city j (each city j being nested within its country i). The slope δ captures the universal elasticity of built mass with respect to population across all neighborhoods, and ε_{ijk} is the neighborhood-level error term.

Identification is achieved by constraining $\sum_i \gamma_i = 0$ and $\sum_{j \in i} \gamma_j = 0$, so that γ_0 remains the grand intercept on the log scale.

We estimate this high-dimensional fixed-effect regression via dummy-variable (within) transformation: first subtracting country and city means to partial out γ_i and γ_j , then fitting δ by ordinary least squares on the demeaned log-population and log-mass. Standard errors are clustered at the city level to allow for arbitrary spatial correlation within each city. Because the outcome and predictor are both in logs, the estimated $\hat{\delta} < 1$ directly quantifies sublinearity: a 1 % increase in local population corresponds to only a $\hat{\delta}$ % increase in built mass, uniformly across all countries and cities. We further validate robustness by fitting the analogous mixed-effects model with random intercepts u_i and u_j , obtaining virtually identical estimates of δ .

Simulation of the emergence of city-level scaling from neighborhood-level disparity

We developed a simulation framework to investigate how variations in the neighborhood-level Zipf's law distribution of population (characterized by the Zipf shape parameter s) influence city-level scaling patterns, given a fixed neighborhood-level scaling exponent ($\delta = 0.75$). The total built mass (M) of cities was modeled as the sum of neighborhood-level built masses (m_i), where $m_i = n_i^\delta$ and n_i is the population of the i -th neighborhood. With these simulated cities, we then estimated the scaling coefficient (β) relating M to N using log-log regression.

To explore the emergent relationship between s and β , we performed a parameter sweep of s values and analyzed the city-level scaling patterns across a range of scenarios. This approach revealed how the aggregation of neighborhood-level power-law distributions affects the observed scaling exponent at the city level. To examine the uncertainties of β , we introduced two random processes: 1) we drew a random s parameter from a normal distribution, centered at the given s with the standard deviation (0.59) estimated from the observed distribution (Fig.3A inset; Fig.4A); 2) we grouped the cities randomly into "countries" by Dirichlet distribution with shape parameter of 0.1 to generate a power-law like distributions of countries ranked by numbers of cities. By applying these two random processes, we produce a distribution of theoretical β values.

Derivation city-level scaling law from neighborhood-level disparity

We partition each city into K standard hexagonal neighborhoods, labeling them so that $n_{(1)}$ is the largest neighborhood population, $n_{(2)}$ the second largest, and so on and so forth. Likewise, $m_{(1)}$ is the largest

neighborhood built mass, $m_{(2)}$ the second largest, etc. Empirical evidence suggests these quantities follow Zipf-like rank–size laws:

$$n_{(i)} \sim i^{-s_n}$$

and

$$m_{(i)} \sim i^{-s_m}$$

where the negative exponents s_n and s_m indicate that population and built mass decrease with increasing rank i . If we posit that the same neighborhood that ranks i -th in population on average also ranks i -th in built mass, we connect these scalings to obtain:

$$m_{(i)} \sim i^{-s_m} = \left(i^{-s_n}\right)^{\frac{s_m}{s_n}} = \left(n_{(i)}\right)^{\frac{s_m}{s_n}}$$

Defining a new parameter

$$\delta = \frac{s_m}{s_n}$$

δ is thus the neighborhood-level scaling exponent relating built mass to population:

$$m_{(i)} \sim n_i^\delta$$

If $s_m < s_n$, then $\delta < 1$, implying sublinear growth of $m_{(i)}$ with $n_{(i)}$.

Note that in this rank-order formulation, s_n is the neighborhood version of Zipf’s city rank-order parameter (31). Empirical evidence suggests that city-level s are frequently found very close to 1 (0.8-1.2). Based on our analysis, the neighborhood level data (Fig.4A) has a Zipf parameter s_n in the range between 0.7 (25% quantile) to 1.4 (75% quantile).

In our dataset, s_m is consistently smaller than s_n , indicating neighborhood-level mass is more homogenous (in the limit case, $s = 0$ represents all neighborhoods are exactly equal in size, the higher the s , the more disparate) than neighborhood-level population distribution.

We then define the total city population

$$N = \sum_{i=1}^K n_i$$

and total city built mass

$$M = \sum_{i=1}^K m_i,$$

and write

$$M \sim N^\beta,$$

where β is the city-level scaling exponent. If $s_n \gg 1$, the largest population $n_{(1)}$ dominates N , and similarly if $s_m \gg 1$ the largest built mass $m_{(1)}$ dominates M . Then

$$N \approx n_{(1)}, \quad M \approx m_{(1)} \sim (n_{(1)})^\delta,$$

so

$$M \sim N^\delta \implies \delta = \beta.$$

Conversely, if s_n is close to zero, so that all neighborhoods are similar in size, then we typically have $N \sim K$. If s_m is close to zero as well, we will have $M \sim K$ too, giving:

$$M \sim N \implies \beta = 1.$$

Hence, β are bounded between δ (in a largest-neighborhood-dominated regime) and 1 (in a homogenous regime).

Figures

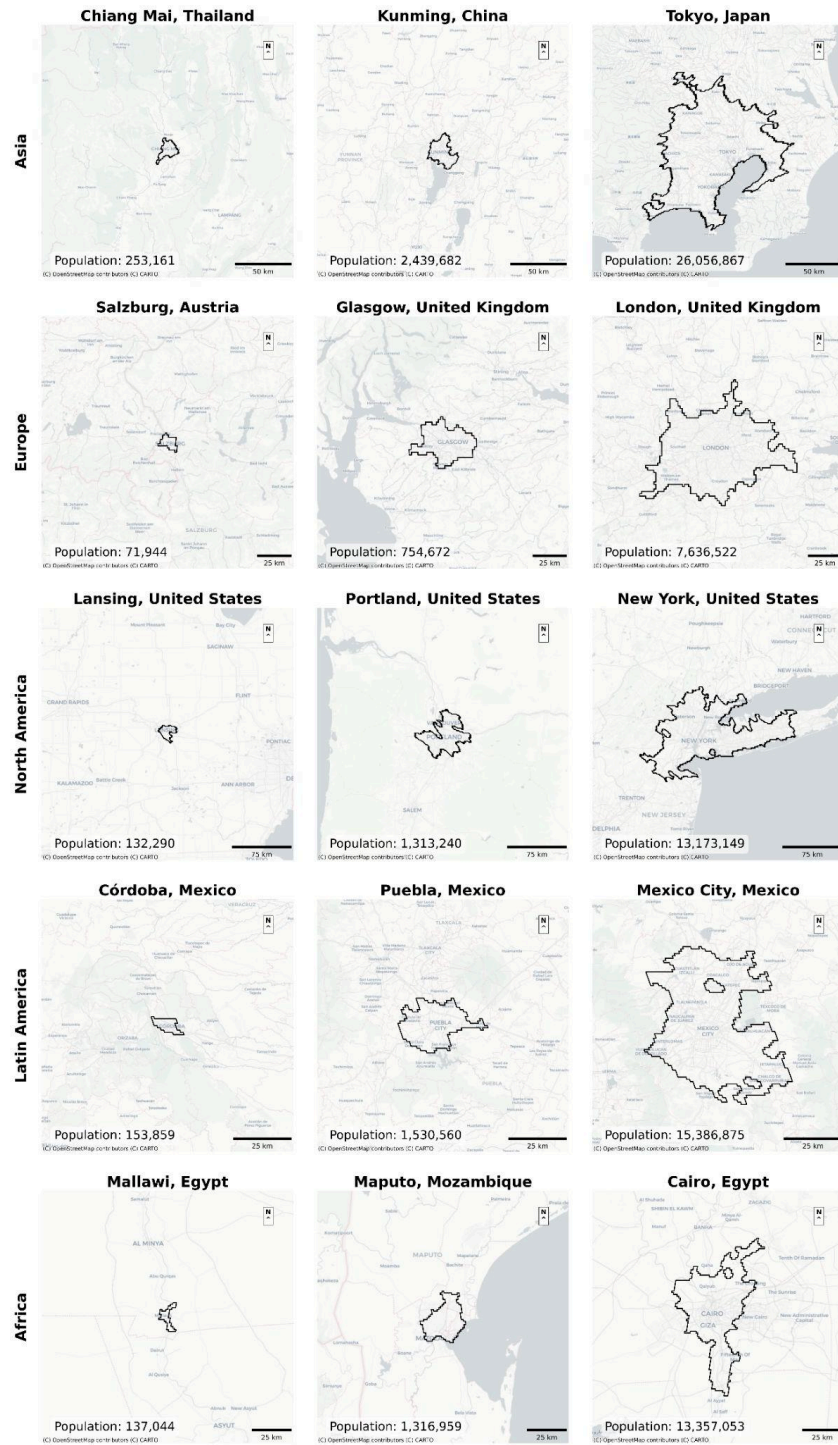


Fig. S1| Illustration of city definition, example cities across various continents demonstrating different scales of cities.

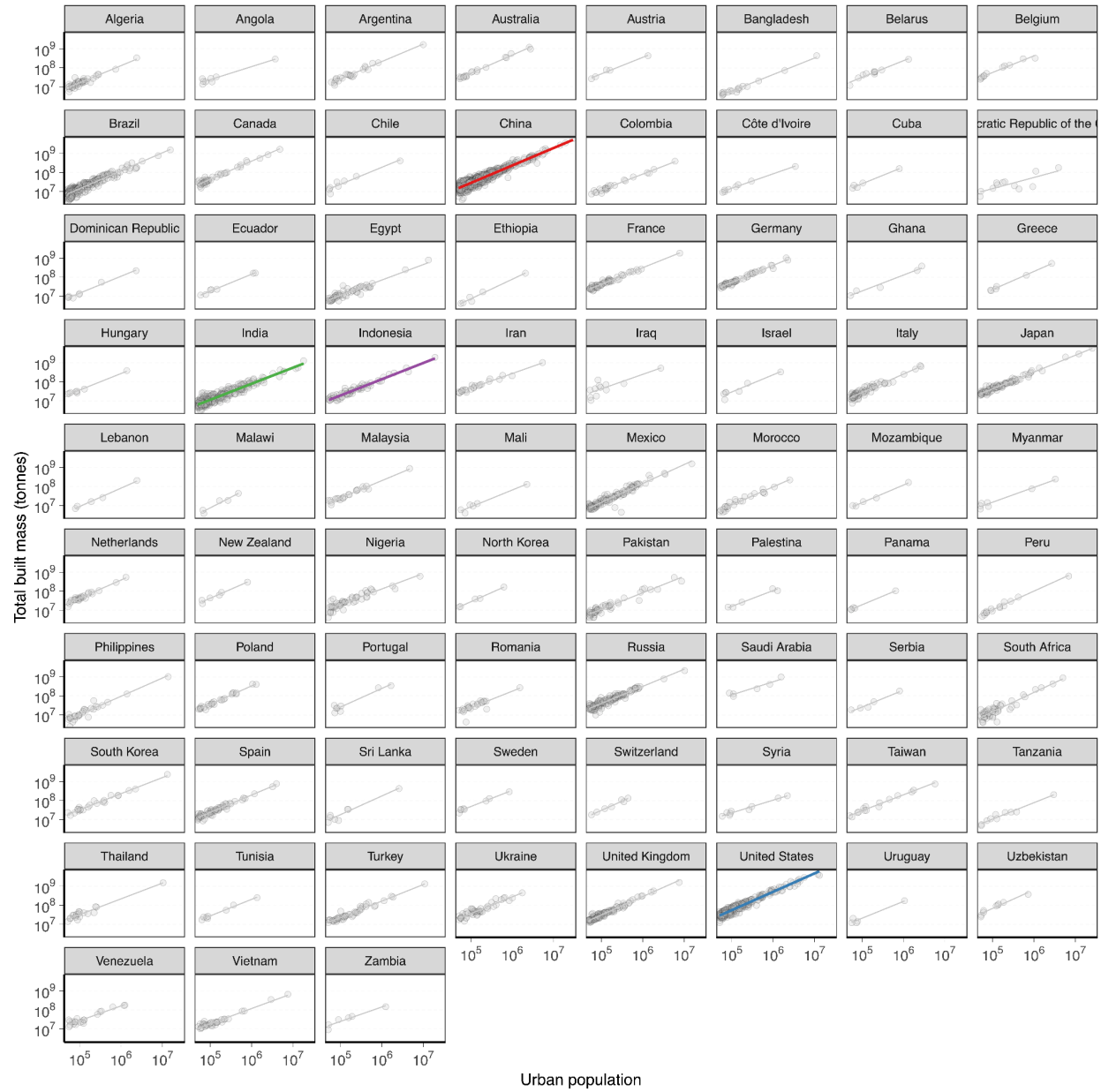


Fig.S2 Sublinear urban scaling of built mass and variations across all countries. We have 74 countries meeting our criteria of inclusion ($n_{\text{cities}} > 5$).

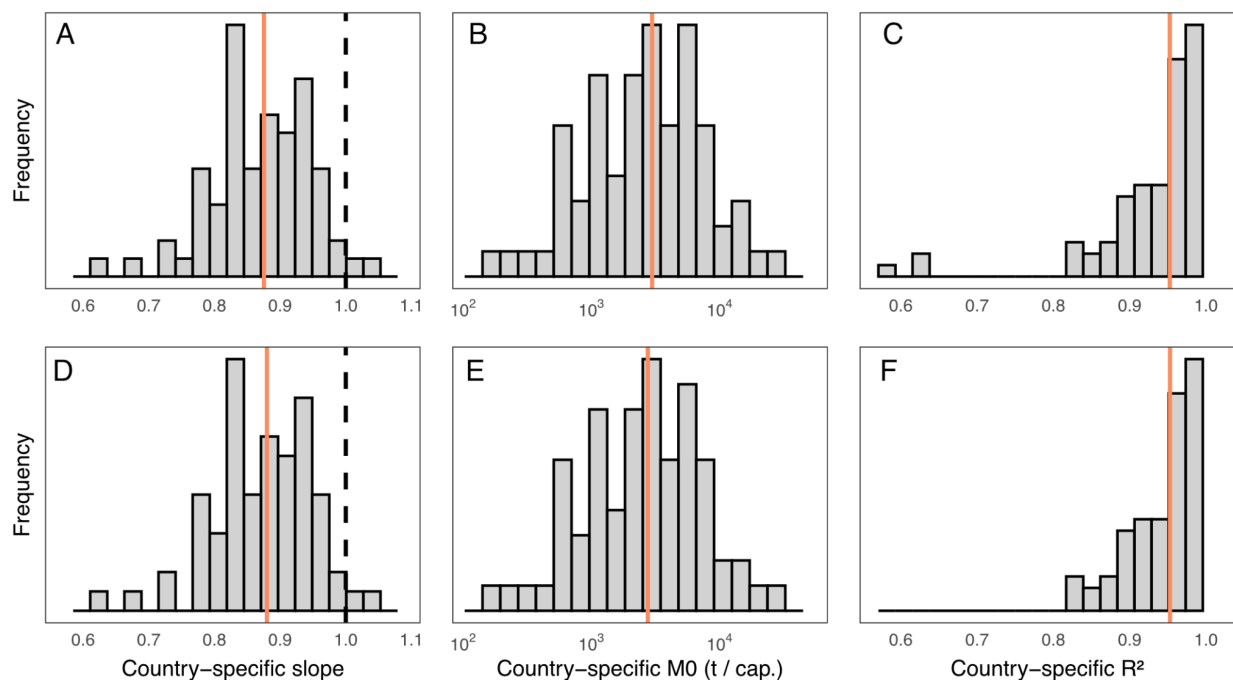


Fig.S3. Country-level scaling analysis stats. The top row (A,B,C) includes all 74 countries with more than 5 cities, while the second row (D,E,F) excludes 3 countries with R^2 lower than 70%. The overall country-level stats are not sensitive to the inclusion of these 3 countries with relatively low goodness of fit.

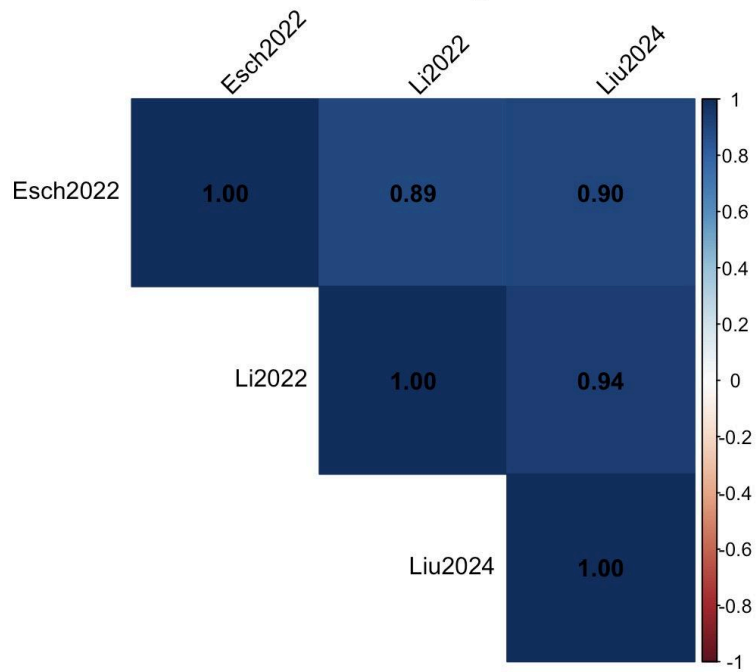


Fig.S4. Correlation matrix of building mass estimates across three global datasets. The heatmap shows Pearson correlation coefficients between city-level building mass estimates from Esch2022, Li2022, and Liu2024 datasets. Analysis includes cities with complete data across all three datasets ($n=3721$).

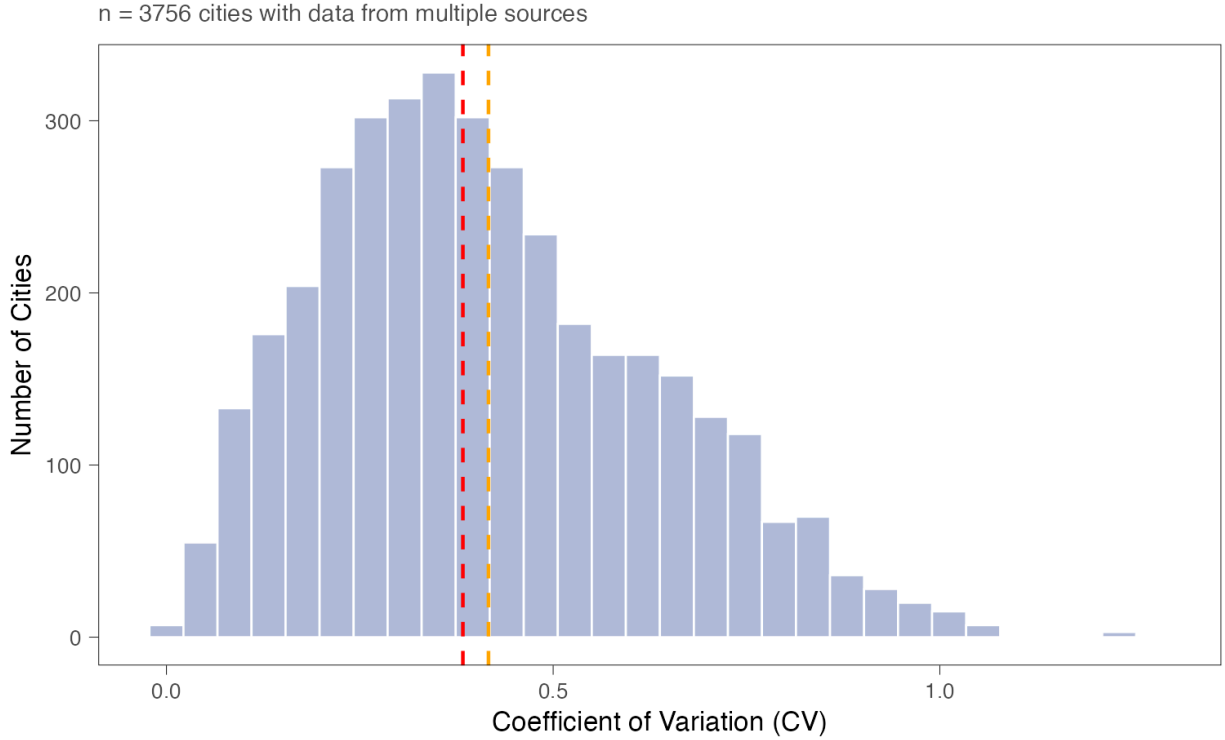


Fig.S5: Distribution of coefficient of variation (CV) of urban building mass estimates across cities from multiple data sources. This histogram illustrates the distribution of the coefficient of variation (CV) of urban building mass estimates across cities, calculated from three global building volume datasets: Esch et al. (2022), Li et al. (2022), and Liu et al. (2024). The CV is derived as the ratio of standard deviation to mean building mass for each city, quantifying the relative variability between different data sources. Only cities with data available from at least two sources are included in the analysis (Zahedan, Iran is the only city with one source and thus excluded from variability analysis). The red dashed line indicates the median CV, while the orange dashed line represents the mean CV.

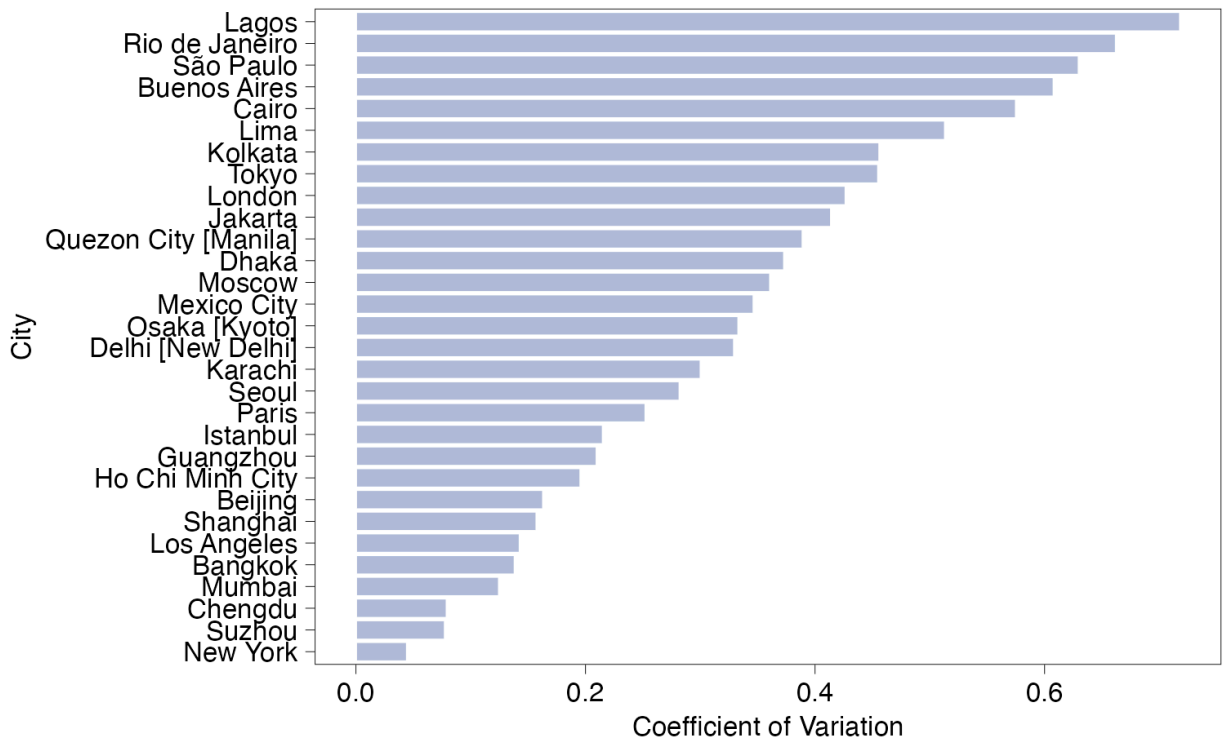


Fig.S6: Coefficient of variation in urban building mass estimates for the 30 most populous cities with multi-source data. Cities are ranked by CV magnitude, showing the relative variability in building mass estimates between the three global datasets (Esch et al. 2022, Li et al. 2022, and Liu et al. 2024). Higher values indicate greater disagreement between data sources for that particular city. Cities are selected based on 2015 population data and represent the largest urban areas where building mass estimates are available from multiple sources.

**SI Table 1 | global summary of various built stock vs. human, vegetation table
(source data for figure 1c)**

Submitted as a separate SI file (Fig1_BoxplotData_20250705.csv), also available on figshare depository.

SI Table 2 | By country scaling analysis slope and intercept

Submitted as a separate SI file (country_summary_table.csv), also available on figshare depository.

SI Table 3 | by city scaling analysis slope and intercept (source data for figure 3)

Submitted as a separate SI file (city_inset_slope_2025-07-05.csv), also available on figshare depository.

References

1. E. Elhacham, L. Ben-Uri, J. Grozovski, Y. M. Bar-On, R. Milo, Global human-made mass exceeds all living biomass. *Nature* **588**, 442–444 (2020).
2. S. A. Spawn, C. C. Sullivan, T. J. Lark, H. K. Gibbs, Harmonized global maps of above and belowground biomass carbon density in the year 2010. *Sci. Data* **7**, 112 (2020).
3. M. Lu, L. O. Hedin, Global plant–symbiont organization and emergence of biogeochemical cycles resolved by evolution-based trait modelling. *Nature Ecology & Evolution* **3**, 239–250 (2019).
4. M. Melchiorri, M. Pesaresi, A. J. Florczyk, C. Corbane, T. Kemper, Principles and applications of the Global Human Settlement Layer as baseline for the Land Use Efficiency indicator—SDG 11.3.1. *ISPRS Int. J. Geoinf.* **8**, 96 (2019).
5. A. Cattaneo, S. Girgin, R. de By, T. McMenomy, A. Nelson, S. Vaz, Worldwide delineation of multi-tier city–regions. *Nat Cities* **1**, 469–479 (2024).
6. M. Lu, C. Zhou, C. Wang, R. B. Jackson, C. P. Kempes, Worldwide scaling of waste generation in urban systems. *Nat Cities* **1**, 126–135 (2024).
7. J. Bousquin, Discrete Global Grid Systems as scalable geospatial frameworks for characterizing coastal environments. *Environ. Model. Softw.* **146**, 1–14 (2021).
8. B. Goodall, *The Penguin Dictionary of Human Geography* (Penguin Books, Harlow, England, 1987).
9. T. Esch, E. Brzoska, S. Dech, B. Leutner, D. Palacios-Lopez, A. Metz-Marconcini, M. Marconcini, A. Roth, J. Zeidler, World Settlement Footprint 3D - A first three-dimensional survey of the global building stock. *Remote Sens. Environ.* **270**, 112877 (2022).
10. M. Li, Y. Wang, J. F. Rosier, P. H. Verburg, J. van Vliet, Global maps of 3D built-up patterns for urban morphological analysis. *Int. J. Appl. Earth Obs. Geoinf.* **114**, 103048 (2022).
11. X. Liu, X. Wu, X. Li, X. Xu, W. Liao, L. Jiao, Z. Zeng, G. Chen, X. Li, Global mapping of three-dimensional (3D) urban structures reveals escalating utilization in the vertical dimension and pronounced building space inequality. *Engineering (Beijing)*, doi: 10.1016/j.eng.2024.01.025 (2024).
12. H. Haberl, A. Baumgart, J. Zeidler, F. Schug, D. Frantz, D. Palacios-Lopez, T. Fishman, Y. Peled, B. Cai, D. Virág, P. Hostert, D. Wiedenhofer, T. Esch, Weighing the global built environment: High-resolution mapping and quantification of material stocks in buildings. *J. Ind. Ecol.* **29**, 159–172 (2025).
13. X. Huang, J. Yang, W. Wang, Z. Liu, Mapping 10 m global impervious surface area (GISA-10m) using multi-source geospatial data. *Earth Syst. Sci. Data* **14**, 3649–3672 (2022).
14. L. S. A. Rousseau, B. Klooststra, H. AzariJafari, S. Saxe, J. Gregory, E. G. Hertwich, Material stock and embodied greenhouse gas emissions of global and urban road pavement. *Environ. Sci. Technol.* **56**, 18050–18059 (2022).
15. D. Frantz, F. Schug, D. Wiedenhofer, A. Baumgart, D. Virág, S. Cooper, C. Gómez-Medina, F. Lehmann, T. Udelhoven, S. van der Linden, P. Hostert, H. Haberl, Unveiling patterns in human dominated landscapes through mapping the mass of US built structures. *Nat. Commun.* **14**, 8014 (2023).

16. D. R. Thomson, D. R. Leasure, T. Bird, N. Tzavidis, A. J. Tatem, How accurate are WorldPop-Global-Unconstrained gridded population data at the cell-level?: A simulation analysis in urban Namibia. *PLoS One* **17**, e0271504 (2022).
17. Z. Bai, J. Wang, M. Wang, M. Gao, J. Sun, Accuracy assessment of multi-source Gridded Population distribution datasets in China. *Sustainability* **10**, 1363 (2018).
18. G. B. West, *Scale: The Universal Laws of Growth, Innovation, Sustainability, and the Pace of Life in Organisms, Cities, Economies, and Companies* (Penguin, 2017).
19. G. Galilei, *Dialogues Concerning Two New Sciences* (Dover, 1914).
20. K. J. Niklas, S. T. Hammond, On the interpretation of the normalization constant in the scaling equation. *Front. Ecol. Evol.* **6** (2019).
21. D. S. Glazier, Commentary: On the Interpretation of the Normalization Constant in the Scaling Equation. *Frontiers in Ecology and Evolution* **8** (2020).
22. J. A. Thomson, On Growth and Form. *Nature* **100**, 21–22 (1917).
23. T. J. Horder, “D’arcy Wentworth Thompson, On growth and form, (1917)” in *Landmark Writings in Western Mathematics 1640-1940* (Elsevier, 2005), pp. 823–832.
24. M. Kleiber, Body size and metabolism. *Hilgardia* (1932).
25. J. Huxley, *Problems of Relative Growth* (Dover, 1972).
26. L. M. A. Bettencourt, J. Lobo, D. Helbing, C. Kühnert, G. B. West, Growth, innovation, scaling, and the pace of life in cities. *Proc. Natl. Acad. Sci. U. S. A.* **104**, 7301–7306 (2007).
27. L. M. A. Bettencourt, Introduction to Urban Science. [Preprint] (2021). <https://doi.org/10.7551/mitpress/13909.001.0001>.
28. L. M. A. Bettencourt, The origins of scaling in cities. *Science* **340**, 1438–1441 (2013).
29. P. Kaitaniemi, How to derive biological information from the value of the normalization constant in allometric equations. *PLoS One* **3**, e1932 (2008).
30. H. Lumer, The Relation between b and k in Systems of Relative Growth Functions of the Form $y = bx^k$. *Am. Nat.* **70**, 188–191 (1936).
31. G. K. Zipf, Human behavior and the principle of least effort: An introduction to human ecology. (1949).